Novel anti-somatostatin receptor 2 antibody-drug conjugate for neuroendocrine cancer therapy

Yingnan Si[1#], Rachael Guenter[1#], Jianfa Ou[1], Seulhee Kim[1], Patrick Ernst[1], Angela M. Carter[2], James A. Bibb[2,5], James M. Markert[3,5], Renata Jaskula-Sztul[2,5], Lufang Zhou[4], Herbert Chen[2,5], and Xiaoguang "Margaret" Liu[1,5*]

[1]*Department of Biomedical Engineering, University of Alabama at Birmingham (UAB), 1825 University Blvd, Birmingham, AL 35294, USA*
[2]*Department of Surgery, UAB, 1808 7th Avenue South, Birmingham, AL 35294, USA*
[3]*Department of Neurosurgery, UAB, 510 20th Street South, Birmingham, AL 35294, USA*
[4]*Department of Medicine, UAB, 703 19th Street South, Birmingham, AL 35294, USA*
[5]*O'Neal Comprehensive Cancer Center, UAB, 1824 6th Avenue South, Birmingham, AL 35233, USA*

[*]Corresponding author: Dr. Xiaoguang "Margaret" Liu, Department of Biomedical Engineering, University of Alabama at Birmingham, 1825 University Blvd., Birmingham, AL 35294, USA. Tel: +001 205-996-1042; Fax: +001 205-996-4701. Email: mliu@uab.edu

[#] These authors contributed equally to this work.

The authors have declared that no conflict of interest exists.

ABSTRACT

Neuroendocrine (NE) cancers include a diverse spectrum of hormone-secreting neoplasms that arise from the endocrine and nervous systems. Current chemo- and radio- therapies have marginal curative benefits. This study aimed to develop an innovative antibody-drug conjugate (ADC) to effectively treat NE tumors (NETs). We first confirmed that somatostatin receptor 2 (SSTR2) is an ideal surface target by analyzing 38 patient-derived NET tissues, 33 normal organs, and 3 NET cell lines. We then developed a new monoclonal antibody (mAb, IgG1 and kappa) to target two extracellular domains of SSTR2, which showed strong and specific surface binding to human and mouse NETs *in vitro* and/or *in vivo*. The ADC was constructed by conjugating the anti-SSTR2 mAb and antimitotic monomethyl auristatin E. *In vitro* evaluations indicated that the ADC can effectively bind, internalize, release payload, and kill NET cells effectively. Finally, ADC was evaluated *in vivo* using a NET xenografted mouse model to determine cancer targeting, maximal tolerated dosage, pharmacokinetics, and anti-cancer efficacy. The anti-SSTR2 ADC can exclusively target and kill NETs with minimal toxicity and high circulation stability. This study has demonstrated that the developed anti-SSTR2 mAb-based ADC has high therapeutic value for NET therapy.

Keywords: neuroendocrine cancers, somatostatin receptor 2, monoclonal antibody, antibody-drug conjugate, targeted therapy

INTRODUCTION

Neuroendocrine (NE) cancers, such as carcinoids, pancreatic islet cell tumors, and medullary thyroid cancer (MTC) (1) arise from cells within the neuroendocrine system that often harbor inherited or sporadic genetic mutations (2). It has been reported that in the United States there is an excess of 100,000 patients living with NE tumors (NETs), there are at least 16,000 new diagnoses each year, and there is an estimation of more than 200,000 undiagnosed cases (3, 4). Patients living with untreatable NET liver metastases have a 5-year survival rate of 13-54% (5). NETs are considered rare, consequentially leading to a lack of insight into their biology and prospective therapy development research; therefore, patients with NETs have limited therapeutic options (6).

Surgical resection alone is often curative for early-stage disease with localized tumors, but 40-95% of patients with NETs are metastatic at the time of initial diagnosis (3, 7-10) (11), making complete resections nearly impossible. Other forms of therapies, including chemoembolization, radioembolization, radiofrequency ablation, cryoablation, and chemotherapy (e.g., mTOR inhibitor "everolimus" and multikinase inhibitor "sunitinib"), have shown limited efficacy and can cause severe systemic toxicities (12-21). Several somatostatin receptor (SSTR)-targeting analogs (e.g., octreotide and lanreotide) have been developed to treat NETs (22), but the clinical data has shown that patients with rapidly proliferating tumors have a relatively poor response to these analogs (23). Thus, it is imperative to develop new treatment strategies such as a targeted therapy.

Somatostatin receptors (SSTRs) are transmembrane proteins that belong to the G-protein coupled receptor (GPCRs) family and are responsible for translating extracellular signals to intracellular responses (24). SSTRs can bind to two somatostatin variants (SST-14 and SST-28) to regulate various neurological and endocrine functions (25). Many patients with NETs overexpress

SSTRs subtype 1 through 5 (SSTR1-5), and the SSTR2 subtype is predominately found on NET cell membrane in 70-100% of cases (26-28). More specifically, the membrane expression level of SSTR2 in NET cells is approximately 20-fold higher than that in normal cells (26-28), which was also confirmed by an immunohistochemistry (IHC) analysis performed on a patient tissue microarray (TMA) and multiple normal organ TMA in this study. Furthermore, it has been reported that SSTR2 is involved in the regulation of cell proliferation and hormone generation-related intracellular signaling pathways in NE cancers (29-36). Therefore, SSTR2 is a potential target for the development of a new targeted therapeutic approach to treat NETs.

Various targeted therapies (37-43), such as monoclonal antibodies (mAbs), antibody-drug conjugates (ADCs), signal transduction inhibitors, and apoptosis inducers have been applied to treat solid tumors while minimizing side effects on normal cells. However, none of these therapies have been developed or applied for NET treatment. Therapeutic mAbs can extend the survival of cancer patients by blocking the cell proliferation or activating the immune response, but can rarely eliminate cancer cells due to their relatively weak cytotoxicity (44). To improve the cytotoxicity, antibody-drug conjugates (ADCs) have been developed by integrating the advantages of mAbs and small molecule chemotherapeutics. The mAb of ADC can specifically bind a tumor-associated surface receptor with low immunological rejection, long plasma half-life, high stability, and minimal side effects (45), while the small molecule portion is toxic to cells. The mAb enables ADC to circulate through the bloodstream until it binds to the tumor specific surface antigen. After receptor binding, the ADC is internalized via receptor-mediated endocytosis and forms a late endosome. Then, lysosomal degradation or linker cleavage (46) occurs to release the cytotoxic drug from the endosome into the cytoplasm of cancer cells (47). Two FDA approved ADCs (i.e., brentuximab vedotin and trastuzumab emtansine) have been developed to treat relapsed Hodgkin

lymphoma, systemic anaplastic large cell lymphoma, and relapsed or chemotherapy refractory HER2-positive breast cancer (48). To our knowledge, neither mAb nor ADC has yet been developed for NET treatment.

The objective of this study was to develop an innovative targeted therapy, i.e. an antibody-drug conjugate, to treat SSTR2-overexpressing NETs. A surface receptor analysis of multiple patient tissues and normal organ tissues showed that SSTR2 is highly expressed in >70% of NET patients. A new anti-SSTR2 mAb was developed and demonstrated as an efficient NET-targeting and drug delivery vehicle, and this mAb was used to conjugate with monomethyl auristatin E (MMAE) to construct an ADC. The specific targeting, maximal tolerated dosage, pharmacokinetics, and anti-cancer efficacy of the anti-SSTR2 ADC were investigated, either *in vitro* using NET cell lines or *in vivo* using NET xenografted mouse models. The results show that the ADC was capable of specifically targeting and effectively killing NET cells.

RESULTS

SSTR2 is overexpressed in NET patient tumor tissues, but not in normal organs. To evaluate the expression level of SSTR2 on the cell surface of NET tissues of patients, an immunohistochemical (IHC) staining analysis was performed on a tissue microarray (TMA). The TMA consisted of 38 formalin-fixed, paraffin-embedded cores of pancreatic NETs from different patients (columns 2-9 in Figure 1), and 5 cores of normal, non-cancerous tissues, including spleen, liver, prostate, placenta and tonsil, as negative controls (column 1 in Figure 1). The TMA was first stained using hematoxylin and eosin (H&E) which indicated the presence and location of the NET cells in each core (Figure 1A). The IHC staining demonstrated that approximately 71% of the patient cores were

positive for SSTR2 with strong cell membrane localization (Figure 1B). Furthermore, the expression of SSTR2 was seen exclusively in the NET tissues, but not detectable in the 5 normal tissues.

The Human Atlas Project (https://www.proteinatlas.org/ENSG00000180616-SSTR2/tissue) database reported a high level of SSTR2 mRNA in the brain, lung, liver, muscles, skin, placenta, prostate, tonsil, and pancreas. A high-level mRNA does not always correlate to a high expression of protein while the surface expression of SSTR2 is more important to develop targeted therapy. Therefore, we investigated the protein expression of SSTR2 in these normal tissues and other normal tissues with IHC staining using our anti-SSTR2 mAb. A commercial multiple-organ TMA (US Biomax, FDA662a, frozen samples) was used in IHC staining, which contains 33 types of normal human tissues, including cerebrum, cerebellum, peripheral nerve, adrenal gland, thyroid gland, spleen, thymus, bone marrow, lymph node, tonsil, pancreas, liver, esophagus, stomach, small intestine, colon, lung, salivary, pharynx, kidney, bladder, testis, prostate, penis, ovary, uterine tube, breast, endometrium, cervix, cardiac muscle, skeletal muscle, mesothelium, and skin. As illustrated in Figures 2A, there is no detectable SSTR2 expression in most normal human tissues except pancreas and skin showing weak positive signal (Figure 2A and Table 1). The high-resolution images of brain, liver, lung, muscle, skin, tonsil, prostate, and pancreas in Figure 2B clearly show the minimal or undetectable surface SSTR2 receptor. As a positive control, the NET patient tissues showed positive and strong signal using our mAb compared to the normal tissues.

Furthermore, we also confirmed the high level of SSTR2 expression in NET cell lines. The quantitative Western blotting analysis showed a high-level expression of SSTR2 in two pancreatic NET cell lines (BON-1 and QGP-1) and a pulmonary NET cell line (H727), but there was minimal

expression in non-cancerous, fibroblast cell lines (917 and WI-38) (Supplementary Figure 1A). Moreover, confocal laser scanning microscopy (CLSM) also revealed strong membrane positivity of SSTR2 in both BON-1 xenografts and NET patient tissues (Supplementary Figure 1B). All the data collected from patient tumor tissues, normal organs, and cell lines suggest that SSTR2 is an ideal target for NET therapy.

Anti-SSTR2 mAb to target NETs. To effectively target the surface receptor SSTR2 in NETs, we developed a mouse anti-human SSTR2 mAb targeting the 1st extracellular domain (cQTEPYYDLTSNA, aa 33-44) and 2nd extracellular domain (cALVHWPFGKAICRVV, aa 104-118) using hybridoma technology. The anti-SSTR2 mAb-producing hybridoma subclones were first screened based on antibody titer using enzyme-linked immunosorbent assays (ELISA). The top 40 clones were ranked based on mAb's binding efficiency to the 1st domain and 2nd domain of SSTR2 (Figure 3A). We selected 4 clones for further evaluation, including Clone 1 that had the strongest binding to the 2nd domain, but had low binding to the 1st domain; Clone 2 which had the highest binding to the 1st domain but low binding to the 2nd domain; and Clones 3 and 4 that had high binding to both the 1st and 2nd extracellular domains.

The anti-SSTR2 mAbs produced by these 4 clones were further evaluated by testing their surface binding to NET cell lines. An isotype analysis showed that Clones 1-4 are IgG1 kappa, IgG2a kappa, IgG1 kappa, and IgG1 kappa, respectively. To define the lead clone, we compared and ranked the capacity of each mAb's binding capacity to the SSTR2 in BON-1 cells using flow cytometry. As shown in Figure 3B, the surface binding percentage of Clones 1-4 was 50%, 80%, 90% and 98%, respectively. A sodium dodecyl sulfate polyacrylamide gel electrophoresis (SDS-PAGE) analysis confirmed that the corresponding anti-SSTR2 mAbs produced from these four clones have a molecular weight around 150 kDa (Figure 3C). Based on the results of mAb

expression and SSTR2-specific binding capability, Clone 4 was selected as the best clone and therefore defined as "lead clone". As presented in Figure 3D, further evaluation showed that the lead anti-SSTR2 mAb had high surface binding to NET cell lines BON-1 and QGP-1 (>90%) and low binding to fibroblast cell lines 917 and WI-38 (<7.5%). Additionally, we and GenScript Inc. isolated, cloned, sequenced, and confirmed that we developed a new anti-SSTR2 mAb (provisional patent TH Docket No. 222119-8030). Therefore, this lead hybridoma clone was used throughout the remainder of this study for a large-scale mAb production and ADC construction.

To optimally scale up and produce a high-quality anti-SSTR2 mAb, we adapted the hybridoma cells from adherent culture in T-flask to suspension culture in spinner flask and stirred-tank bioreactor. The mAb production was performed in Gibco Hybridoma-SFM medium supplemented with 6 g/L glucose, 6 mM L-glutamine, 3.5 g/L Cell Boost #6, and 1% anti-clumping agent (v/v) (Figure 3E). The cultures in T-flask, spinner flask, and stirred-tank bioreactor generated 8.6, 39.8, and 53.3 mg/L of anti-SSTR2 mAb with a specific growth rate of 0.016, 0.024 and 0.035 h^{-1}, respectively (Figure 3F). The anti-SSTR2 mAb was purified following our previously reported procedure (49, 50).

Anti-SSTR2 mAb showed high surface binding to NETs both in vitro and in vivo. To assess the *in vitro* NET-specific targeting of the anti-SSTR2 mAb to SSTR2, we performed dynamic live-cell CLSM imaging and flow cytometry using NET cell lines. To visualize and track the surface binding process, we transfected BON-1 cells with BacMam GFP control and conjugated an Alexa Fluor 647 dye (AF647, labeled as red color, ex./em. 650/665 nm) to the anti-SSTR2 mAb. As shown in Figure 4A, the anti-SSTR2 mAb accumulated on the BON-1 cell surface due to the immunoaffinity, displayed as a "red circle", at 20 mins after incubating mAb with cells. The mAb was then internalized by endocytosis and localized in cytoplasm within 40 mins. We also compared

the surface binding capability of the developed mAb versus a commercially available mAb (R&D Systems) using flow cytometry. As described in Figure 4B, the mAb developed in this study had much stronger surface binding to BON-1 cells as compared to the commercial mAb, 95% vs. 38%, under the same staining conditions. In addition, the confocal imaging showed that the anti-SSTR2 mAb bound to and was completely internalized by PanNET cell line (BON-1) and MTC cell lines (TT and MZ-CRC-1) within 70 mins post-incubation (Figure 4C).

Furthermore, we evaluated the *in vivo* targeting capability of the anti-SSTR2 mAb using NET xenografted mouse model. The mouse model bearing BON-1-Luc cells transfected with firefly luciferase, a bioluminescent reporter. IVIS imaging at 4-8 hrs post-mAb injection indicated a strong accumulation of Cy7-mAb in the BON-Luc xenografts, but there was also a marginal amount of mAb remaining in the murine circulation system. Imaging at 24 hrs demonstrated complete co-localization of the bioluminescent signal from the BON-Luc xenografts and the fluorescent signal from the Cy7-mAb (Figure 5A). The BON-Luc xenograft, liver, and brain were collected and sectioned to test the mAb binding using CLSM. It is found that there was no detectable non-specific binding of Cy7-mAb to liver or brain, but there was a strong fluorescent signal detected on a section of the BON-Luc xenograft (data not shown). Altogether, both *in vitro* and *in vivo* studies conducted herein have confirmed that the developed anti-SSTR2 mAb can target the SSTR2-overexpressing NET cell lines, xenografts, and patient tissues. Therefore, it is evident that the new mAb has the potential to target and deliver highly potent small molecules in the form of an ADC.

Anti-SSTR2 mAb detects both human and mouse SSTR2. In humans, SSTR2 is endogenously expressed on the cell membrane as a glycoprotein with four extracellular domains, seven helical transmembrane domains, and four cytoplasmic domains (51-53). As summarized in

Table 2, the UniProtKB database showed that isoform A of human SSTR2 (UniProt P30874) and mouse SSTR2 (UniProt P30875) have the same topology. Our mouse anti-human SSTR2 mAb was generated using the 1st and 2nd extracellular domains from the human SSTR2, that both have 100% similarity with mouse SSTR2. With this design, we expect that our anti-SSTR2 mAb can detect both human and mouse SSTR2. To test this hypothesis, Western blotting was performed, showing that our anti-SSTR2 mAb can detect SSTR2 present in BON-1 xenografts and in isolated medullary thyroid carcinoma (MTC) cells from a spontaneous MTC mouse model (Figure 5C). This MTC model was previously developed as the first reliable and clinically accurate conditional MTC mouse model (54, 55). The bi-transgenic mouse line was engineered to allow doxycycline dependent repression of p25 (p25OE) under the control of neural specific enolase (NSE) promoter. This study showed that the anti-SSTR2 mAb can detect both human and mouse SSTR2 receptor.

ADC construction and characterization. We employed our established and reported platform of a cysteine-based conjugation procedure (49) to construct ADC. Herein, the rebridging peptide-based linker was synthesized to maintain high integrity of the mAb (Figure 6A), conjugated with antimitotic monomethyl auristatin E (MMAE), and purified using Waters high-performance liquid chromatography (HPLC). The structure of linker was characterized using Agilent 6500 Q-TOF LC/MS (Figure 6B), and the integrity of ADC structure was confirmed using SDS-PAGE (Figure 6C). The average drug-antibody ratio (DAR) of the constructed ADC was approximately 4.0.

In vitro anti-cancer toxicity of anti-SSTR2 ADC showed a low IC_{50}. We evaluated the *in vitro* anti-cancer toxicity of the anti-SSTR2 ADC in BON-1 cells by comparing free drug (MMAE) and two different ADCs that included either the mAb developed in this study or the mAb from R&D Systems. MMAE was selected as the drug for the ADC due to the fact it is a potent cytotoxin

that has already been clinically validated (56, 57) as a microtubulin polymerization blocking agent (58, 59). However, MMAE has never been tested in NETs. In this study, the IC_{50} values of MMAE, ADC from our anti-SSTR2 mAb, and ADC from the commercial mAb were 2.00 nM, 4.27 nM, and 5.62 nM, respectively (Figure 6D). It is clear that mAb-MMAE ADC has similar nanomolar cytotoxicity to NET cells as the highly potent free drug MMAE. With strong NET-targeting capability, our mAb-based ADC is expected to achieve better treatment efficacy *in vivo* than free drug.

Anti-SSTR2 ADC has multiple potential anti-cancer mechanisms. To understand other potential anti-cancer mechanisms of the anti-SSTR2 ADC in addition to the cytotoxicity caused by the delivery of MMAE, we analyzed several markers associated with cell proliferation signaling pathways in BON-1 cells treated with the ADC for three days. Western blot showed that both anti-SSTR2 mAb alone and ADC can block cell proliferation signaling via the PI3K-AKT pathway, downregulate the oncogene Cyclin D1, and induce cell cycle arrest as seen by the detection of the marker p21 (Figure 6E). Our studies found that the ADC released MMAE inhibited NET cell proliferation by microtubule de-polymerization (Figure 6F).

Moreover, we also tested the possible effect of our anti-SSTR2 mAb on cytokine production in $CD8^+$ T cells. Post CD3/CD28 stimulation, human $CD8^+$ T cells were incubated with either 100 nM of SST analog (Octreotide) or 100 nM of the anti-SSTR2 mAb for 2 days. After incubation, flow cytometry was performed to analyze the expression of IL-2 and IFN-γ. As shown in Supplementary Figure S2, both the anti-SSTR2 mAb and Octreotide increased IL-2 expression by 1.6 folds and IFN-γ expression by 2.2 folds. Further investigation should be done to examine the level of cytokines *in vivo* after treatment with the anti-SSTR2 mAb and the anti-SSTR2 ADC in future.

In summary, we propose several possible mechanisms of action for anti-SSTR2 ADC treatment of NETs (Supplementary Figure S3). The first mechanism is that the anti-SSTR2 mAb functions as a targeting delivery vehicle of drug to NET cells and the drug payload inhibits cancer cells proliferation via depolymerizing microtubulin. The second potential mechanism is that the PI3K-AKT proliferative signaling pathway is downregulated by the mAb binding and consequent blockage of SSTR2. The third potential mechanism is that the cytokine production of T cells is enhanced by the anti-SSTR2 mAb. The contribution of these mechanisms needs to be further investigated and defined through additional *in vitro* and *in vivo* studies using multiple NET cell lines, xenografts, and transgenic animal models.

MTD of the anti-SSTR2 ADC showed no side effects. To investigate the maximum tolerated dose (MTD) of the anti-SSTR2 ADC, 5 different concentrations were injected into the tail vein of 5 wild-type (non-tumor bearing) mice: 4, 8, 12, 16, and 20 mg/kg of body weight (BW). Mice were monitored at six hours post-injection and twice daily for a total of 21 days and showed no signs of behavior changes such as water intake, labored breathing, rapid weight loss, impaired ambulation, and/or mentation. As shown in Figure 7A, ADC at a concentration range of 4-20 mg/kg BW had no obvious side effects on mice body weight or overall survival. After monitoring for a total of three weeks, mice were sacrificed and brain tissue was collected for further studies. As shown in H&E staining (Figure 7B), the brain tissue was not morphologically altered after the administration of the anti-SSTR2 ADC. There is no obvious drug delivery and no any signs of acute or chronic inflammation or any apoptotic or necrotic regions was observed. These results suggest that the anti-SSTR2 ADC treatment had no evident off-target effects and did not cause detectable damage to the brain *in vivo*.

PK indicated high stability of the anti-SSTR2 ADC. Preliminary pharmacokinetic (PK) studies were done by intravenously injecting the ADC into mice bearing subcutaneous NET xenograft at five different concentrations: 4, 8, 12, 16, and 20 mg/kg BW (n=4). Plasma samples were collected for PK analysis (10-50 µL each) from the tail vein at time points of: 0 hr, 2 hrs, 8 hrs, 16 hrs, 1 day, 2 days, 3 days, 5 days, and 7 days post-ADC injection and then titrated using an ELISA assay (Figure 7C). As presented in Table 3 the PK modeling demonstrated the calculated half-life ($t_{1/2}$) = 1.38-2.33 days, volume of distribution V_d = 63.05-94.42 mL/kg, the clearance rate (C_L) = 28.01-37.45 mL/days/kg, bioavailability (F) = 568.58-1293.26%, recommended dose (D) = 3.78-14.30 mg/kg BW, and recommended dosing interval (τ) = 4.40-9.10 days. Based on these results, we selected a concentration of 8 mg/kg BW and a dosing interval of 4-5 days for the remaining anti-cancer *in vivo* studies.

In vivo anti-cancer efficacy of anti-SSTR2 ADC. The mice bearing BON-Luc xenografts were treated in a dosing interval of 4.5 days with either: the anti-SSTR2 ADC at a concentration of 8 mg/kg, saline as a vehicle control, and anti-SSTR2 mAb (control, 8 mg/kg) in three groups (n=6). Figure 8A shows that tumor growth was significantly inhibited with a tumor size reduction of 62-67% in the mice treated with the anti-SSTR2 ADC as compared with the controls. The tumor fluorescence flux was also measured with the IVIS imaging system and showed a reduction of 71-73% of tumor growth in the ADC treated group compared to control groups (Figure 8B). The NET tumors were collected in the end of the study (Figure 8C), and the wet weight also confirmed the significant inhibition of tumor growth (Figure 8D). There was no obvious difference among the three groups in overall body weight (Figure 8E). A Western blotting analysis showed that SSTR2 expression was present in NET tumors during treatment (Figure 8F). The surface staining of SSTR2 in tumors from ADC treatment group appeared to be lower than the staining seen in the

control group (Figure 8G), likely due to the NET cell death caused by ADC which was confirmed through H&E staining (Figure 8H). This *in vivo* anti-cancer efficacy study demonstrated that the anti-SSTR2 mAb is a good drug delivery vehicle and the antibody-drug conjugate can effectively inhibit NET growth.

DISCUSSION

SSTR2 receptor is an ideal NET target. To develop effective and safe targeted cancer therapies, a unique biomarker that specifically defines the cancer cells from the non-cancerous cells must be identified and thoroughly characterized. As reported in this study, SSTR2 is overexpressed in approximately 70% of 38 patients with NETs. Other studies also have reported that 70-100% of NETs abundantly express SSTR2 on the cell surface (26-28). Although it has been reported that SSTR2 can be normally expressed in the central nervous system (CNS), gastrointestinal (GI) tract, and pancreas (60), the expression of SSTR2 in NET tissues was observed to be >20-fold higher than normal tissues in a tissue microarray using IHC analysis as described in this study and literature (26-28). Considering that the mAb-based ADC is a dose-dependent targeted therapy, the drastic difference in SSTR2 expression between NETs and other tissues assures that it can be safe to exploit SSTR2.

However, not all patients with NETs overexpress SSTR2 (61, 62). It has been reported that 45-66% of patients with pulmonary NETs (61) and 80-95% patients with gastroenteropancreatic NETs express SSTR2. The tissue microarray analysis performed in this study showed that out of the 38 patient tissues stained, only about 71% showed detectable SSTR2 expression. In order to benefit the patients that lack a high expression of SSTR2, we have begun to identify other potential

surface markers in NETs, such as carcinoembryonic antigen-related cell adhesion molecule 1 (CEACAM1), using comparative membrane proteomics and Western blotting (data not shown). We have found that CEACAM1 has high expression in two pancreatic NET cell lines (BON-1 and QGP-1) and no expression in neither pancreatic adenocarcinoma cell lines (PANC-1 and MiAPaCa-1) nor a fibroblast cell line (WI-38). Other studies also have reported CEACAM1 expression in various other cancers, including medullary thyroid cancer cell lines which represent a type of NET (63, 64). This finding indicated that we could potentially use CEACAM1 as an alternative of SSTR2 for the NET patients with minimal SSTR2 density although it needs a full evaluation in future study.

Our anti-SSTR2 mAb is an effective drug delivery vehicle. This study demonstrated that SSTR2 is an appropriate target for NET therapy. Differently from the commercial anti-SSTR2 mAb developed using the whole SSTR2 membrane protein as an immunogen, the new anti-SSTR2 mAb developed in this study was created using two extracellular domains of SSTR2 as immunogens. Therefore, it showed a binding capability to NET cells over 5 times greater than that of the commercially available anti-SSTR2 mAb. Sequencing of the anti-SSTR2 mAb developed herein confirmed its novelty (provisional patent TH Docket No. 222119-8030).

The Human Atlas Project reported high mRNA level of SSTR2 in multiple normal human tissues, but the surface protein expression level of SSTR2 is our main consideration for targeted cancer therapy, rather than transcription level. This study analyzed multiple normal human organ tissue arrays (total of 33 organs), including most of the reported tissues with high mRNA, confirming the low or undetectable SSTR2 protein expression on the cell surface of these tissues. The live-animal IVIS imaging demonstrated that our anti-SSTR2 mAb exclusively accumulated in the NET xenograft. Since our mAb can target both human and mouse SSTR2, the *in vivo* specific

targeting to NET in mouse models can indicate the specific targeting in patients. Additionally, we evaluated the possible toxicity of anti-SSTR2 ADC on mice and specifically brain tissue. The MTD data showed that a dose of up to 20 mg ADC/kg BW did not cause any body weight or behavior changes of the mice. Importantly, H&E staining on murine brain tissue did not show any evidence of damage or changes in cellular morphology. Therefore, we can conclude that our anti-SSTR2 mAb is a potentially safe drug delivery vehicle.

Innovative targeted therapy to effectively treat NETs. The mTOR inhibitor (Everolimus), multikinase inhibitor (Sunitinib), and SST analogs (e.g., Octreotide and Lanreotide) have been developed to treat NETs (12-22), but these drugs have limited therapeutic efficacy. In this study, for the first time, we developed a SSTR2-targeted therapy in the form of a monoclonal antibody-drug conjugate to target NETs. The ADC has advantages that include: enhanced cellular uptake via strong surface binding, high cytotoxicity of the small molecule payload that is delivered to cancer cells, and minimal side effects. Our *in vivo* anti-cancer efficacy study demonstrated that tumor growth was significantly reduced upon treatment with the anti-SSTR2 ADC, which suggests that our mAb can effectively target NET cells and deliver the conjugated toxic drug. Moreover, we suspect that our anti-SSTR2 mAb can be used to tag the surface of liposomes and exosomes to facilitate the targeted delivery of other drugs. The single-chain variable fragment (scFv) can also be cloned to construct CAR-T cells for immunotherapy of NETs.

Synergistic therapy of anti-SSTR2 mAb and anti-SSTR2 ADC. Other studies have reported multiple direct and indirect mechanisms that could drive anti-tumor effects mediated by SSTR2. For example, the direct anti-proliferation mechanisms include apoptosis (65), regulation of cyclin-dependent kinase inhibitors, and the inhibition of proliferation signaling (66). The potential indirect anti-tumor effects include the inhibition of growth factor and hormone release, anti-

angiogenic effects (67), and immune response regulation (36). The *in vitro* evaluation done in this study showed that our anti-SSTR2 mAb downregulates PI3K/AKT signaling which is associated with cell proliferation, downregulates the expression of the oncogene cyclin D1, upregulates p21 expression which is associated with cell cycle arrest, and activates $CD8^+$ T cells by increasing cytokine production. These findings indicate that this anti-SSTR2 mAb-based ADC could serve as a novel multi-purpose biologic with clinical potentials such as: directly causing cell death by releasing a cytotoxic payload into the cellular cytoplasm, inhibiting tumor cell growth cia the SSTR2-mediated modulation of signaling cascades, and re-activating T cell function by increasing cytokine production. Further investigation is necessary to better understand the possible synergy of anti-SSTR2 mAb and ADC for NET treatment *in vivo* using a sporadic MTC mouse model, humanized mouse model, and liver metastasis mouse model.

Impact of our targeted therapy and future work. Our anti-SSTR2 ADC has advantages over traditional chemotherapy, radiotherapy, and surgery to treat metastatic NE cancers. Compared to surgical procedures, anti-SSTR2 ADC can target and treat the metastatic nodules. Compared to chemotherapy, this therapy can reduce undesirable side effects and improve the anti-cancer therapeutic efficacy. Similar to other receptors that are FDA-approved for targeted therapies, SSTR2 is not an absolute NET-specific receptor, so it is imperative to further evaluate the potential side effects. The combination of the facts that SSTR2 expression in NETs is greater than normal tissues, SSTR2 has little or undetectable surface expression in most normal organs, and that the ADC is a dosage-dependent treatment strategy could minimize possible off-target side effects. Combined with other therapies, the targeted therapy developed in this study has great potential to improve the quality of life and survival rate of patients with NE cancers.

METHODS

NET patient tissue microarray (TMA) to analyze receptor expression. A tissue microarray was prepared by the university Research Pathology Core. Patient tissues were obtained from the university Surgical Oncology Tumor Bank through an Institutional Review Board (IRB) approved protocol. The TMA consisted of thirty-eight pancreatic neuroendocrine patient tissue cores and five negative control cores including tissues from the liver, spleen, placenta, prostate, and tonsil. All tissues were paraffin-embedded.

Multiple human organ normal tissue array to analyze SSTR2 distribution. The 33 organs tissue microarray slides (Catalog#: FDA662a) were purchased from US Biomax (Rockville, MD). IHC straining (procedure was described in details in the following section) was performed to analyze the cell surface SSTR2 expression in these organs. The 33 organs are cerebrum, cerebellum, peripheral nerve, adrenal gland, thyroid gland, spleen, thymus, bone marrow, lymph node, tonsil, pancreas, liver, esophagus, stomach, small intestine, colon, lung, salivary， pharynx, kidney, bladder， testis, prostate, penis, ovary, uterine tube, breast, endometrium, cervix, cardiac muscle, skeletal muscle, mesothelium, and skin. As positive control, NET patient tissues were also stained at the same conditions using our developed anti-SSTR2 mAb.

NET cell lines and seed cultures. Multiple human NET cell lines, including BON-1 (pancreatic NET), QGP-1 (pancreatic NET), BON-1 cell line carrying a firefly luciferase reporter gene (BON-Luc), MZ-CRC-1 (thyroid NET), and TT (thyroid NET), were used for *in vitro* or *in vivo* studies. The BON-1 and MZ-CRC-1 cell lines were maintained in DMEM/F12 basal medium supplemented with 10% fetal bovine serum (FBS) and 4 mM L-glutamine; the TT cell line was maintained in RPMI-1640 supplemented with 20% FBS and 4 mM L-glutamine. The non-

cancerous negative control cell lines, including WI-38 (pulmonary fibroblast) and 917 (foreskin fibroblast), were maintained in MEM-E medium supplemented with 10% FBS, 1% non-essential amino acids, and 1% sodium pyruvate. All cell lines were incubated in either T25 or T75 flasks at 37 ^{o}C and 5% CO_2 in a humidified incubator (Caron, Marietta, OH). The cell growth, i.e. viable cell density (VCD) and viability, were measured using Countess II automated cell counter ortrypan blue (Thermo Fisher Scientific, Waltham, MA). All basal media, supplements, and reagents used in this study were purchased from Thermo Fisher Scientific or Life Technologies (Part of Fisher) unless otherwise specified.

Hybridoma cell lines and seed cultures. The adherent culture of anti-SSTR2 mAb producing hybridoma clones were maintained in DMEM supplemented with 10% FBS in T flasks, which was used for clone evaluation in flow cytometry and confocal microscopy imaging. To produce large-scale mAb in stirred-tank bioreactor, we adapted top four hybridoma clones from adherent culture to serum-free suspension culture and cultivated cells in Hybridoma-SFM medium supplemented with 4 mM L-glutamine and 1% anti-clumping agent (v/v) in shaker flasks at 37 ^{o}C, 5% CO_2 and 130 rpm.

Anti-SSTR2 mAb development. Both human SSTR2 (isoform A, UniProtKB P30874) and mouse SSTR2 (isoform A, UniProtKB P30875) are an integral membrane glycoprotein with the same topology, including four extracellular topological domains, seven helical transmembrane, and four cytoplasmic topological domains. Protein blast analysis showed that the four extracellular domains have similarity of 81%, 100%, 100%, and 90%, respectively. To develop a monoclonal antibody that can target both human and mice SSTR2, we developed an anti-human SSTR2 mAb to target the 1st extracellular domain (cQTEPYYDLTSNA, aa 33-44) and the 2nd extracellular domain (cALVHWPFGKAICRVV, aa 104-118) using hybridoma technology. The synthesized

antigen peptides were intravenously (i.v.) injected into five balb/c mice for immunization and boosts every two weeks for ten weeks (five injections), which was performed by ProMab following standard protocol. The anti-SSTR2 mAb in the sera collected from the immunized mice, both pre-immune serum and anti-SSTR2 serum, was titrated using antigen peptides-based sandwich enzyme-linked immunosorbent assay (ELISA) and Western blotting. The immune splenocytes from the mouse with the best anti-SSTR2 antibody titer was fused with myeloma cells (Sp2/0) to obtain hybridoma clones.

mAb producing hybridoma clones screening. Total of 100 subclones were generated, cultivated in 96-well plates during the first two stages of screenings. The primary clone screening was performed based on SSTR2 mAb volumetric productivity (i.e. final titer) using mixed double domains of antigen, which generated the top 40 clones. In the secondary screening, the top 4 clones were screened using peptide (1^{st} or 2^{nd} extracellular domain)-based ELISA. In the tertiary screening, we adapted the top four clones in serum-free suspensive cultures and performed batch culture in shaker flask. The mAb was purified using Protein A kit and labeled with AF647 following the manufacturing protocol to evaluate cancer surface binding in flow cytometry and confocal microscopy imaging. The lead clone with strong surface binding to NET (BON-1) cells and low binding to non-cancerous H727 control cells was defined for further evaluation and ADC construction.

ELISA. ELISA was used in the early stage immunization and hybridoma clone screening. Briefly, 96-well plates were coated with antigen diluted in 50 mM carbonate at pH 9.6 and incubated overnight at 4 ^{o}C. The spent medium containing mAb or the purified mAb diluted in blocking buffer was added at 100 µL each well and incubated for 1 hr at room temperature (RT). The anti-SSTR2 mAb was captured and detected by adding 50 µL each well of HRP-labeled anti-

mouse IgG (Sigma, St. Louis, MO, Catalog#: RABHRP2-10UL) diluted to 1:10,000 in blocking buffer. The buffer A containing 0.1 M $Na_3C_6H_5O_7 \cdot 2H_2O$ and 1.5% $CH_4N_2O \cdot H_2O_2$ and buffer B containing 3,3',5,5'-tetramethylbenzidine and 0.1 M $C_6H_8O_7 \cdot H_2O$ were used for color development. The plates were read at 450 nm on microplate reader after adding stop solution.

Isotype evaluation. The commercial mouse antibody isotyping kit was used to determine the isotype of the developed mAb. Specifically, the goat anti-mouse IgG, IgA and IgM were used to coat plate. After adding mAb samples, the subclass specific rabbit anti-mouse IgG1, IgG2a, IgG2b, IgG3, IgA, IgM, κ and λ were added. The HRP labeled anti-rabbit IgG and substrate solution were used to develop color.

Anti-SSTR2 mAb production. The lead SSTR2 mAb producing hybridoma clone was maintained in 125-mL shaker flask. The seed train was scaled up to 3-L spinner flask with working volume of 1 L and agitation 80 rpm. The mAb production was performed in a 5-L stirred-tank bioreactor cell culture that was controlled at Temp 37 °C, pH 7.0, DO 50% and agitation 70 rpm. Specifically, the batch production culture in bioreactor was seeded with VCD of 0.3-0.5 $x10^6$ cells/mL in Hybridoma-SFM supplemented with 6 g/L glucose, 6 mM L-glutamine, 3.5 g/L Cell Boost #6, and 1% anti-clumping agent. The production cultures were sampled daily to monitor the cell growth (i.e., VCD, viability, double time, and growth rate) using cell counter, glucose using glucose analyser, and mAb production using NGC system (Bio-Rad, Hercules, CA). When viability dropped to around 80%, the spent medium was harvested and clarified using centrifuge and 0.22 μm ultrafiltration for further purification of mAb.

mAb purification. Our previously developed protocol of two-step antibody purification (49, 50) using NGC system was used to purify the anti-SSTR2 mAb. Specifically, the primary Protein A affinity purification was performed to capture mAb in a UNOsphere SUPrA column which was

equilibrated with a buffer comprised of 0.02 M sodium phosphate and 0.02 M sodium citrate at pH 7.5. After column washing, mAb was eluted with buffer containing 0.02 M sodium citrate and 0.1 M sodium chloride at pH 3.0 and neutralized to 7.0 with 1 M Tris solution. The polishing purification was performed using a cation exchange column Foresight Nuvia S and the mAb was eluted using 20 mM to 200 mM sodium chloride solution. The purified mAb was titrated using NGC and characterized using SDS-PAGE, Western blotting, flow cytometry, and confocal microscope as described in the following sections.

ADC construction. Our published platform of cysteine-based conjugation procedure (49) was used to construct ADC. First, rebridging linker was synthesized by mixing 6-aminohexanoic acid with 3,4-dibromofuran-2,5-dione at a 1:1 molar ratio at 60 ^{oC} for 30 mins, heated at 100 ^{o}C for 18 hrs, and purified by silica gel with 0-40% dichloromethane/ethyl acetate as eluent solution. Second, N,N'-diisopropylcarbodiimide, N,N-diisopropylethylamine, and rebridging linker were mixed in dichloromethane with a molar ratio of 1:1:2.5 for 1 hr at 25 ^{o}C. Then identical molarity of MMAE was added and frequently mixed for 16 hrs to synthesize linker-payload which was purified through HPLC system (Waters, Milford, MA) equipped with a reversed-phase C18 column with 5 μm C18(2) 100Å and 250 x 10 mm (Phenomenex, Torrance, CA). Third, anti-SSTR2 mAb exchanged to 50 mM borate buffer (pH 8.0) and MMAE were conjugated with molar ratio of 1:7 and purified through PD SpinTrap^{TM} G25 columns (GE Healthcare). Finally, the average drug-antibody ratio (DAR) was calculated as Ratio = $(\varepsilon_{Ab}^{248}-R\varepsilon_{Ab}^{280})/(R\varepsilon_{D}^{280}-\varepsilon_{D}^{248})$, where $R = A_{248}/A_{280}$ = Absorbance ratio (49), and confirmed using liquid chromatography-electro-spray ionization-tandem mass spectrometry (LC-ESI-MS).

In vitro anti-cancer toxicity (IC_{50}). BON cell line was utilized to compare the toxicity of ADC. 75 uL of culture media containing cells (viability > 95%) with a density of $5x10^4$ cells/mL

was added in each well of 96-well plate. ADC or MMAE solution was sterilized by 0.2 μm filter and diluted to different concentrations with complete medium. After 4-hr incubation in regular cell culture incubator, 75 uL of ADC or MMAE with gradient concentrations were mixed with cells in the 96-well plate. The well plate was covered by another 96-well plate filled with PBS to prevent medium evaporation during treatment period. After 3-day incubation, the toxicity result was generated through Luminescent Cell Viability Assay (Promega, Madison, MI).

SDS-PAGE and Western blotting. The Mem-PER plus membrane protein extraction kit was used to extract membrane proteins for surface receptor evaluation. The protein concentration was determined by the Pierce BCA assay following manufacturing protocol. Non-reducing SDS-PAGE was run using electrophoresis system with NuPAGE™ 4-12% Bis-Tris protein gels. The gel proteins were electro-transferred to a PVDF membrane and blocked with TBS washing buffer containing 5% fat-free milk powder and 0.1% Tween 20 for 1 hr at RT. The primary rabbit anti-mouse antibody (Abcam, Cambridge, MA, Catalog#: ab190475) with 1:5,000 dilution from 1 mg/mL stock was incubated with the blocked membrane overnight at 4 ^{o}C, rinsed three times with TBS buffer, and then incubated with HRP-conjugated secondary anti-rabbit antibody (Abcam, catalog#: ab205718)) with dilution of 1:3,000 for 1 hr at RT. Finally the blotted membrane was treated with Luminata Forte Western HRP substrate (Millipore, Boston, MA), imaged with MyECL imager, and quantified with ImageJ software.

Flow cytometry to quantitate surface receptor density and mAb binding. The purified anti-SSTR2 mAb was labelled with an Alexa Fluor™ 647 Antibody Labelling Kit and used to quantitatively evaluate the surface receptor binding capacity to NET cell lines (BON, TT and MZ) and negative control fibroblast cell line (917) using a BD LSRII flow cytometer (BD Biosciences, San Jose, CA). We harvested 1 x10^6 cells from T-flasks when confluence reached 70%, washed

with flow cytometry buffer, and incubated with 1 μg AF647 labeled mAb on ice or RT in darkness for 30 mins. After washing three times, the cells were re-suspended in 1 mL of flow cytometer buffer, and analyzed with BD Biosciences' BD LSRII flow cytometer. Gating was set where negative sample has <0.5% fluorescent population. As control, the commercial anti-SSTR2 mAb (RD Systems, Minneapolis, MN, Catalog#: MAB4224) was used in flow cytometry.

Confocal imaging to evaluate ADC binding and internalization. The laminin was coated on glass coverslips (Warner Instruments, Hamden, CT) at a concentration of 10 μg/mL to enhance adhesion efficiency and incubated for 24 hrs at 4 ^{o}C. The NET cells or negative cells were seeded onto glass cover slips with a density of $5x10^4$ cells/mL in a 24-well plate, and incubated for 4 hrs at 37 ^{o}C. When cells reached 50% confluence, BacMam GFP Transduction Control was added to transduce cells and incubated overnight, which stain the cytoplasma and nucleus. Next the AF647 labelled mAb was diluted with PBS to a concentration of 2 μg/mL. The coverslips containing transduced cells were then rinsed twice with PBS, transferred to an appropriate micro-incubation stage adapter, and stained with 500 μL of 2 μg/mL AF647-mAb in a PBS buffer containing 10% inactivated goat serum and 1% bovine serum albumin at 37 °C in darkness for 30 mins. The cells were observed using Olympus 1X-81 confocal microscope with Olympus FV-1000 laser scan head using a confocal microscope (Olympus IX81, Center Valley, PA). The MitoSox images were recorded using an Olympus FV1000 confocal microscope to monitor surface binding and internalization of AF647-mAb. A 488 nm laser with 0.2% transmissivity and a PMT voltage of 519 V was used to visualize BacMam infected cells while a 635 nm laser with 31% transmissivity and a PMT voltage of 686 V was used to visualize the fluorescent labeled mAbs. The images were analyzed offline with the ImageJ software.

Xenograft mouse model generation and anti-NET efficacy study. BON-Luc seed culture was tested as mycoplasma-free before scaling up. Cells were concentrated and injected onto the back of each Nude (nu/nu) mice (4-6 weeks of age, male and female) (Jackson Labs) with a density of $1x10^6$ cells/mouse, viability > 95%. Tumors were allowed to grow 5 days post-xenograft. Mice with 50~60 mm^3 tumor volume were selected for ADC efficacy study. Mice were randomized to 3 groups (n=6): saline, anti-sstr2 mAb, mAb-MMAE conjugate. Treatment started on day 6 post injection: mAb/ADC was administrated through tail vein following a dose of 12 mg/kg-BW, 2 injections/week; the same volume of saline was injected in the saline group. The volume of solid tumor and mouse body weight were measured every two days. Four injections were conducted with average injection interval of 4.5 days during the entire treatment period. Mice were sacrificed on Day 28 post-xenograft. Solid tumors and other organs (brain and liver) were collected for imaging and further analysis.

Biodistribution by In Vivo Imaging System (IVIS). Xenograft mouse model was generated using the method above. At the 7^{th} day post-xenograft, mice with 100-150 mm^3 solid tumor were selected for mAb bio-distribution study. The anti-SSTR2 mAb was labeled with fluorescent dye using Sulfo-Cyanine5.5 antibody labeling kit (Lumiprobe). After sterilization, 25 μg of Cy5.5-mAb was injected into each mouse through tail vein. Mice were imaged 24 hrs post-injection under *in vivo* imaging system. Parameter was set up as 660nm/710nm (excitation/emission) wavelength.

Pharmacokinetics study. To investigate the metabolic rate of ADC, 5 different concentrations (4, 8, 12, 16, 20 mg/kg-BW) of ADC were injected to 5 groups of randomized mice (n=4). Blood samples were collected from tails at 2, 5, 24, 48, 72, 120 hrs post-injection (6 time points in total). Blood was centrifuged at 2,000 g for 5 mins to precipitate cells and the supernatant was collected for ELISA analysis. Standard sandwich ELISA was used to quantify the ADC

remained in mouse plasma. SSTR2 peptide was utilized to coat 96-well plates. Horseradish peroxidase conjugated goat-anti mouse IgG antibody and 3,3',5,5'-Tetramethylbenzidine (TMB) were used for color development. The ADC in plasma was diluted and titrated using ELISA with detection range of 0-300 ng/mL. The recommended dose (D) and dosing interval (τ) were calculated using previously developed PK model (Ref): $D = C_{max(desired)} \cdot k_e \cdot V_d \cdot T \cdot (1-e^{-ke\tau})/(1-e^{-keT})$ and $\tau = \ln(C_{max(desired)}/C_{min(desired)})/k_e + T$, which were used in the anti-cancer efficacy animal study.

Hematoxylin and eosin (H&E) staining. The section was deparaffinized before staining. 200 µL of hematoxylin solution was added to stain the section, followed by 5-min incubation at 25 ^{o}C. The dye was washed away by running tap water from reverse side. The section was rinsed in PBS for 5 mins. Then, the section was stained in 400 µL of eosin Y solution for 30 seconds and washed using running tap water. The section was dehydrated in absolute alcohols by two 2-min reactions and cleared in xylene.

Immunohistochemistry (IHC) staining. Formalin-fixed and paraffin-embedded NET tissue were prepared and sectioned by the Tissue-Based Translational Research Lab in the Department of Pathology at UAB. The normal organs TMA was purchased from US, Biomax, Inc. Slides were cleared and rehydrated using xylene and ethanol. Slides were then immersed in citrate buffer (BioGenex, Fermont, CA) for a ten-minute pressure cooker cycle to achieve antigen retrieval. Endogenous peroxidase activity was quenched by incubating slides in 3% hydrogen peroxide for ten minutes. Blocking was performed for 1 hr at RT using 3% goat serum and 0.3% Triton-X100 in PBS. SSTR2 was detected with an overnight 4 °C incubation using 1.8 mg/mL of anti-SSTR2 mAb. An anti-mouse biotin-labeled secondary antibody was used, followed by a 30-min incubation with HRP streptavidin. Slides were stained with DAB Chromogen (Dako Liquid DAB+ substrate K3468) and counter stained with hematoxylin. Before being cover slipped and imaged,

slides were dehydrated and cleared using ethanol and xylene.

Statistics. All the data were presented as mean ± standard error of the mean (SEM). Two-tailed Student's *t* tests were used to determine the significance between two groups. Comparison among multiple groups was performed using a one-way ANOVA followed by post-hoc (Dunnett's) analysis. The sample size of animal study was determined by prior study and published ADC therapy study (68). The statistical significance with ***P value of < 0.001 was considered for all tests.

Study approval. The tumor tissue samples from NET patients were obtained from the UAB Surgical Oncology Tumor Bank through an Institutional Review Board (IRB) approved protocol. Information identifying patient was replaced with sequentially assigned numbers. The normal human organs tissue away was purchased from US Biomax, Inc. Animal studies were conducted in compliance with the Guidelines for the Care and Use of Research Animals established by the UAB IACUC (IACUC-20422).

Author contributions

Y.S., J.O., R.J., L.Z., H.C. and X.L. BL designed experiments. Y.S., R.G., J.O., S.K., and P.E. developed experimental protocols, performed experiments, and analyzed the data. R.J. and H.C. contributed patient samples and aided in NET xenograft animal model development. A.C. and J.B. contributed transgenic animal NET tissues. Y.S. R.G., J. M., and X.L. wrote manuscript. X.L., R.G. L.Z. and H.C. conceived the overall project idea. All authors contributed to manuscript revision.

Acknowledgements

The authors would like to thank Dr. J. Bart Rose and the Tissue-Based Translational Research Lab in the Department of Pathology at UAB for the design and construction of the tissue microarray. Ms. Yun Lu assisted the i.v. injection and organ extraction in animal study. The proteomic analysis was conducted at the UAB Comprehensive Cancer Center Mass Spectrometry/Proteomics (MSP) Shared Facility. This study was supported by the National Institute of Health (Grant Number R21 HL 127599A1, 2016), start-up fund from the University of Alabama at Birmingham (UAB), and North American Neuroendocrine Tumor Society (NANETS) Basic/Translational Science Investigator award.

Reference

1. Yao JC, Hassan M, Phan A, Dagohoy C, Leary C, Mares JE, et al. One hundred years after "carcinoid": epidemiology of and prognostic factors for neuroendocrine tumors in 35,825 cases in the United States. *J Clin Oncol.* 2008;26(18):3063-72.
2. Kulke MH, Benson AB, 3rd, Bergsland E, Berlin JD, Blaszkowsky LS, Choti MA, et al. Neuroendocrine tumors. *J Natl Compr Canc Netw.* 2012;10(6):724-64.
3. Chen H, Hardacre JM, Uzar A, Cameron JL, and Choti MA. Isolated liver metastases from neuroendocrine tumors: does resection prolong survival? *J Am Coll Surg.* 1998;187(1):88-92; discussion -3.
4. Norton JA. Endocrine tumours of the gastrointestinal tract. Surgical treatment of neuroendocrine metastases. *Best Pract Res Clin Gastroenterol.* 2005;19(4):577-83.
5. Mayo SC, de Jong MC, Pulitano C, Clary BM, Reddy SK, Gamblin TC, et al. Surgical management of hepatic neuroendocrine tumor metastasis: results from an international multi-institutional analysis. *Ann Surg Oncol.* 2010;17(12):3129-36.
6. Batcher E, Madaj P, and Gianoukakis AG. Pancreatic neuroendocrine tumors. *Endocrine research.* 2011;36(1):35-43.
7. Adler JT, Meyer-Rochow GY, Chen H, Benn DE, Robinson BG, Sippel RS, et al. Pheochromocytoma: current approaches and future directions. *Oncologist.* 2008;13(7):779-93.
8. Pinchot SN, Pitt SC, Sippel RS, Kunnimalaiyaan M, and Chen H. Novel targets for the treatment and palliation of gastrointestinal neuroendocrine tumors. *Curr Opin Investig Drugs.* 2008;9(6):576-82.
9. Chen H, Pruitt A, Nicol TL, Gorgulu S, and Choti MA. Complete hepatic resection of metastases from leiomyosarcoma prolongs survival. *J Gastrointest Surg.* 1998;2(2):151-5.
10. Chen H. Therapeutic options for patients with metastatic gastrointestinal carcinoid. *J Surg Oncol.* 2008;97(3):203-4.
11. Shiba S, Morizane C, Hiraoka N, Sasaki M, Koga F, Sakamoto Y, et al. Pancreatic neuroendocrine tumors: A single-center 20-year experience with 100 patients. *Pancreatology.* 2016;16(1):99-105.
12. Brown KT, Koh BY, Brody LA, Getrajdman GI, Susman J, Fong Y, et al. Particle embolization of hepatic neuroendocrine metastases for control of pain and hormonal symptoms. *J Vasc Interv Radiol.* 1999;10(4):397-403.
13. Isozaki T, Kiba T, Numata K, Saito S, Shimamura T, Kitamura T, et al. Medullary thyroid carcinoma with multiple hepatic metastases: treatment with transcatheter arterial embolization and percutaneous ethanol injection. *Intern Med.* 1999;38(1):17-21.
14. Eriksson B, Kloppel G, Krenning E, Ahlman H, Plockinger U, Wiedenmann B, et al. Consensus guidelines for the management of patients with digestive neuroendocrine tumors--well-differentiated jejunal-ileal tumor/carcinoma. *Neuroendocrinology.* 2008;87(1):8-19.
15. Lal A, and Chen H. Treatment of advanced carcinoid tumors. *Curr Opin Oncol.* 2006;18(1):9-15.
16. Lehnert T. Liver transplantation for metastatic neuroendocrine carcinoma: an analysis of 103 patients. *Transplantation.* 1998;66(10):1307-12.
17. Zhang R, Straus FH, and DeGroot LJ. Effective genetic therapy of established medullary thyroid carcinomas with murine interleukin-2: dissemination and cytotoxicity studies in a rat tumor model. *Endocrinology.* 1999;140(5):2152-8.

18. Boudreaux JP, Putty B, Frey DJ, Woltering E, Anthony L, Daly I, et al. Surgical treatment of advanced-stage carcinoid tumors: lessons learned. *Ann Surg.* 2005;241(6):839-45; discussion 45-6.
19. Nguyen C, Faraggi M, Giraudet AL, de Labriolle-Vaylet C, Aparicio T, Rouzet F, et al. Long-term efficacy of radionuclide therapy in patients with disseminated neuroendocrine tumors uncontrolled by conventional therapy. *J Nucl Med.* 2004;45(10):1660-8.
20. Fiorentini G, Rossi S, Bonechi F, Vaira M, De Simone M, Dentico P, et al. Intra-arterial hepatic chemoembolization in liver metastases from neuroendocrine tumors: a phase II study. *J Chemother.* 2004;16(3):293-7.
21. Zuetenhorst JM, Valdes Olmos RA, Muller M, Hoefnagel CA, and Taal BG. Interferon and meta-iodobenzylguanidin combinations in the treatment of metastatic carcinoid tumours. *Endocr Relat Cancer.* 2004;11(3):553-61.
22. Oberg K, Kvols L, Caplin M, Delle Fave G, de Herder W, Rindi G, et al. Consensus report on the use of somatostatin analogs for the management of neuroendocrine tumors of the gastroenteropancreatic system. *Ann Oncol.* 2004;15(6):966-73.
23. Sideris L, Dube P, and Rinke A. Antitumor effects of somatostatin analogs in neuroendocrine tumors. *Oncologist.* 2012;17(6):747-55.
24. Ferguson SS. Evolving concepts in G protein-coupled receptor endocytosis: the role in receptor desensitization and signaling. *Pharmacol Rev.* 2001;53(1):1-24.
25. Cakir M, Dworakowska D, and Grossman A. Somatostatin receptor biology in neuroendocrine and pituitary tumours: part 2--clinical implications. *J Cell Mol Med.* 2010;14(11):2585-91.
26. Pinchot SN, Holen K, Sippel RS, and Chen H. Carcinoid tumors. *Oncologist.* 2008;13(12):1255-69.
27. Zatelli MC, Tagliati F, Taylor JE, Rossi R, Culler MD, and degli Uberti EC. Somatostatin receptor subtypes 2 and 5 differentially affect proliferation in vitro of the human medullary thyroid carcinoma cell line tt. *J Clin Endocrinol Metab.* 2001;86(5):2161-9.
28. Sun LC, and Coy DH. Somatostatin receptor-targeted anti-cancer therapy. *Curr Drug Deliv.* 2011;8(1):2-10.
29. Barbieri F, Bajetto A, Pattarozzi A, Gatti M, Wurth R, Thellung S, et al. Peptide receptor targeting in cancer: the somatostatin paradigm. *Int J Pept.* 2013;2013:926295.
30. Pitt SC, Chen H, and Kunnimalaiyaan M. Inhibition of phosphatidylinositol 3-kinase/Akt signaling suppresses tumor cell proliferation and neuroendocrine marker expression in GI carcinoid tumors. *Ann Surg Oncol.* 2009;16(10):2936-42.
31. Pitt SC, Chen H, and Kunnimalaiyaan M. Phosphatidylinositol 3-kinase-Akt signaling in pulmonary carcinoid cells. *J Am Coll Surg.* 2009;209(1):82-8.
32. Pitt SC, Davis R, Kunnimalaiyaan M, and Chen H. AKT and PTEN expression in human gastrointestinal carcinoid tumors. *Am J Transl Res.* 2009;1(3):291-9.
33. Cervia D, Fiorini S, Pavan B, Biondi C, and Bagnoli P. Somatostatin (SRIF) modulates distinct signaling pathways in rat pituitary tumor cells; negative coupling of SRIF receptor subtypes 1 and 2 to arachidonic acid release. *Naunyn Schmiedebergs Arch Pharmacol.* 2002;365(3):200-9.
34. Vedvyas Y, Shevlin E, Zaman M, Min IM, Amor-Coarasa A, Park S, et al. Longitudinal PET imaging demonstrates biphasic CAR T cell responses in survivors. *JCI Insight.* 2016;1(19):e90064.
35. Talme T, Ivanoff J, Hagglund M, Van Neerven RJ, Ivanoff A, and Sundqvist KG. Somatostatin receptor (SSTR) expression and function in normal and leukaemic T-cells. Evidence for

selective effects on adhesion to extracellular matrix components via SSTR2 and/or 3. *Clin Exp Immunol.* 2001;125(1):71-9.
36. Elliott DE, Li J, Blum AM, Metwali A, Patel YC, and Weinstock JV. SSTR2A is the dominant somatostatin receptor subtype expressed by inflammatory cells, is widely expressed and directly regulates T cell IFN-gamma release. *Eur J Immunol.* 1999;29(8):2454-63.
37. Zhou L, Xu N, Sun Y, and Liu XM. Targeted biopharmaceuticals for cancer treatment. *Cancer Lett.* 2014;352(2):145-51.
38. Almasbak H, Aarvak T, and Vemuri MC. CAR T Cell Therapy: A Game Changer in Cancer Treatment. *J Immunol Res.* 2016;2016:5474602.
39. Dai H, Wang Y, Lu X, and Han W. Chimeric Antigen Receptors Modified T-Cells for Cancer Therapy. *J Natl Cancer Inst.* 2016;108(7).
40. Magee MS, and Snook AE. Challenges to chimeric antigen receptor (CAR)-T cell therapy for cancer. *Discov Med.* 2014;18(100):265-71.
41. Zhang BL, Qin DY, Mo ZM, Li Y, Wei W, Wang YS, et al. Hurdles of CAR-T cell-based cancer immunotherapy directed against solid tumors. *Sci China Life Sci.* 2016;59(4):340-8.
42. Kunert R, and Reinhart D. Advances in recombinant antibody manufacturing. *Appl Microbiol Biotechnol.* 2016;100(8):3451-61.
43. Polakis P. Antibody Drug Conjugates for Cancer Therapy. *Pharmacol Rev.* 2016;68(1):3-19.
44. Liu JKH. The history of monoclonal antibody development – Progress, remaining challenges and future innovations. *Annals of Medicine and Surgery.* 2014;3(4):113-6.
45. Little M, Kipriyanov SM, Le Gall F, and Moldenhauer G. Of mice and men: hybridoma and recombinant antibodies. *Immunology Today.* 2000;21(8):364-70.
46. Stump B, and Steinmann J. *Antibody-Drug Conjugates*. Springer; 2013:235-48.
47. Saunders LR, Bankovich AJ, Anderson WC, Aujay MA, Bheddah S, Black K, et al. A DLL3-targeted antibody-drug conjugate eradicates high-grade pulmonary neuroendocrine tumor-initiating cells in vivo. *Sci Transl Med.* 2015;7(302):302ra136.
48. Pereira DS, Guevara CI, Jin L, Mbong N, Verlinsky A, Hsu SJ, et al. AGS67E, an Anti-CD37 Monomethyl Auristatin E Antibody-Drug Conjugate as a Potential Therapeutic for B/T-Cell Malignancies and AML: A New Role for CD37 in AML. *Mol Cancer Ther.* 2015;14(7):1650-60.
49. Ou J, Si Y, Gah KY, Yasui N, Guo Y, Song J, et al. Bioprocess development of antibody-drug conjugate production for breast cancer treatment. *PLOS ONE.* 2018;In review.
50. Xu N, Ou J, Si Y, Goh KYF, D.,, Han S, Yang Y, et al. Proteomics insight into the production of monoclonal antibody. *Biochemical Engineering Journal.* 2018;145:177-85.
51. Yamada Y, Post SR, Wang K, Tager HS, Bell GI, and Seino S. Cloning and functional characterization of a family of human and mouse somatostatin receptors expressed in brain, gastrointestinal tract, and kidney. *Proc Natl Acad Sci U S A.* 1992;89(1):251-5.
52. Petersenn S, Rasch AC, Presch S, Beil FU, and Schulte HM. Genomic structure and transcriptional regulation of the human somatostatin receptor type 2. *Mol Cell Endocrinol.* 1999;157(1-2):75-85.
53. Ota T, Suzuki Y, Nishikawa T, Otsuki T, Sugiyama T, Irie R, et al. Complete sequencing and characterization of 21,243 full-length human cDNAs. *Nat Genet.* 2004;36(1):40-5.
54. Pozo K, Castro-Rivera E, Tan C, Plattner F, Schwach G, Siegl V, et al. The role of Cdk5 in neuroendocrine thyroid cancer. *Cancer Cell.* 2013;24(4):499-511.

55. Pozo K, Hillmann A, Augustyn A, Plattner F, Hai T, Singh T, et al. Differential expression of cell cycle regulators in CDK5-dependent medullary thyroid carcinoma tumorigenesis. *Oncotarget.* 2015;6(14):12080-93.
56. Francisco JA, Cerveny CG, Meyer DL, Mixan BJ, Klussman K, Chace DF, et al. cAC10-vcMMAE, an anti-CD30-monomethyl auristatin E conjugate with potent and selective antitumor activity. *Blood.* 2003;102(4):1458-65.
57. Yao H, Jiang F, Lu A, and Zhang G. Methods to Design and Synthesize Antibody-Drug Conjugates (ADCs). *Int J Mol Sci.* 2016;17(2).
58. Cunningham D, Parajuli KR, Zhang C, Wang G, Mei J, Zhang Q, et al. Monomethyl Auristatin E Phosphate Inhibits Human Prostate Cancer Growth. *Prostate.* 2016;76(15):1420-30.
59. Li H, Yu C, Jiang J, Huang C, Yao X, Xu Q, et al. An anti-HER2 antibody conjugated with monomethyl auristatin E is highly effective in HER2-positive human gastric cancer. *Cancer Biol Ther.* 2016;17(4):346-54.
60. Cakir M, Dworakowska D, and Grossman A. Somatostatin receptor biology in neuroendocrine and pituitary tumours: part 1--molecular pathways. *J Cell Mol Med.* 2010;14(11):2570-84.
61. Righi L, Volante M, Tavaglione V, Bille A, Daniele L, Angusti T, et al. Somatostatin receptor tissue distribution in lung neuroendocrine tumours: a clinicopathologic and immunohistochemical study of 218 'clinically aggressive' cases. *Ann Oncol.* 2010;21(3):548-55.
62. Sherman SK, Maxwell JE, Carr JC, Wang D, O'Dorisio MS, O'Dorisio TM, et al. GIPR expression in gastric and duodenal neuroendocrine tumors. *J Surg Res.* 2014;190(2):587-93.
63. Thies A, Moll I, Berger J, Wagener C, Brummer J, Schulze HJ, et al. CEACAM1 expression in cutaneous malignant melanoma predicts the development of metastatic disease. *J Clin Oncol.* 2002;20(10):2530-6.
64. Tilki D, Irmak S, Oliveira-Ferrer L, Hauschild J, Miethe K, Atakaya H, et al. CEA-related cell adhesion molecule-1 is involved in angiogenic switch in prostate cancer. *Oncogene.* 2006;25(36):4965-74.
65. Guillermet J, Saint-Laurent N, Rochaix P, Cuvillier O, Levade T, Schally AV, et al. Somatostatin receptor subtype 2 sensitizes human pancreatic cancer cells to death ligand-induced apoptosis. *Proc Natl Acad Sci U S A.* 2003;100(1):155-60.
66. Lahlou H, Guillermet J, Hortala M, Vernejoul F, Pyronnet S, Bousquet C, et al. Molecular signaling of somatostatin receptors. *Ann N Y Acad Sci.* 2004;1014:121-31.
67. Woltering EA. Development of targeted somatostatin-based antiangiogenic therapy: a review and future perspectives. *Cancer Biother Radiopharm.* 2003;18(4):601-9.
68. Sherbenou DW, Aftab BT, Su Y, Behrens CR, Wiita A, Logan AC, et al. Antibody-drug conjugate targeting CD46 eliminates multiple myeloma cells. *J Clin Invest.* 2016;126(12):4640-53.

Table Legends

Table 1. Summary of the surface binding of anti-SSTR2 mAb to 33 normal human organ tissues.

Table 2. Anti-SSTR2 mAb targeted 1st and 2nd domains of human SSTR2 and mouse SSTR2.

Table 3. PK modeling parameters.

Table 1. Summary of the surface binding of anti-SSTR2 mAb to 33 normal human organ tissues.

Position	No.	Age	Sex	Organ	Pathology diagnosis	Type	SSTR2 Staining
A1	1	35	M	Cerebrum	Cerebrum tissue	Normal	-
A2	2	24	F	Cerebellum	Cerebellum tissue	Normal	-
A3	3	31	M	Nerve	Peripheral nerve tissue	Normal	-
A4	4	43	M	Adrenal gland	Adrenal gland tissue	Normal	-
A5	5	44	F	Thyroid	Adjacent normal thyroid gland tissue	NAT	-
A6	6	21	F	Spleen	Spleen tissue	Normal	-
A7	7	42	M	Thymus gland	Thymus gland tissue	Normal	-
A8	8	21	F	Bone marrow	Bone marrow tissue	Normal	-
A9	9	25	M	Lymph node	Iymph node tissue and fibrovascular tissue	Normal	-
A10	10	28	M	Tonsil	Tonsil tissue	Normal	-
A11	11	35	F	Pancreas	Pancreas tissue	Normal	±
B1	12	24	F	Cerebrum	Cerebrum tissue	Normal	-
B2	13	35	M	Cerebellum	Cerebellum tissue	Normal	-
B3	14	18	F	Nerve	Peripheral nerve tissue	Normal	-
B4	15	18	F	Adrenal gland	Adrenal gland tissue	Normal	-
B5	16	50	M	Thyroid	Thyroid gland tissue	Normal	-
B6	17	35	M	Spleen	Spleen tissue	Normal	-
B7	18	16	M	Thymus gland	Thymus gland tissue	Normal	-
B8	19	33	M	Bone marrow	Bone marrow tissue	Normal	-
B9	20	40	M	Lymph node	Iymph node tissue	Normal	-
B10	21	21	F	Tonsil	Tonsil tissue	Normal	-
B11	22	50	M	Pancreas	Pancreas tissue	Normal	±
C1	23	56	F	Liver	Adjacent normal liver tissue	NAT	-
C2	24	15	F	Esophagus	Esophagus tissue	Normal	-
C3	25	38	M	Stomach	Stomach tissue	Normal	-
C4	26	35	M	Small intestine	Small intestine tissue	Normal	-
C5	27	35	M	Colon	Colon tissue	Normal	-
C6	28	35	M	Lung	Lung tissue	Normal	-
C7	29	45	M	Salivary gland	Salivary gland tissue	Normal	-
C8	30	62	M	Larynx	Larynx tissue	AT	-
C9	31	47	M	Kidney	Kidney tissue	Normal	-
C10	32	22	M	Bladder	Bladder tissue	Normal	-
C11	33	28	M	Testis	Testis tissue	Normal	-
D1	34	38	M	Liver	Liver tissue	Normal	-
D2	35	45	M	Esophagus	Esophagus tissue	Normal	-
D3	36	50	M	Stomach	Stomach tissue	Normal	-
D4	37	25	M	Small intestine	Small intestine tissue	Normal	-
D5	38	35	M	Colon	Colon tissue	Normal	-
D6	39	48	M	Lung	Lung tissue	Normal	-
D7	40	54	F	Salivary gland	Adjacent normal salivary gland tissue	NAT	-
D8	41	43	M	Larynx	Pharynx tissue	Normal	-
D9	42	38	M	Kidney	Kidney tissue	Normal	-
D10	43	50	M	Bladder	Bladder tissue	Normal	-
D11	44	30	M	Testis	Testis tissue	Normal	-
E1	45	31	M	Prostate	Prostate tissue	Normal	-
E2	46	35	M	Penis	Penis tissue	Normal	-
E3	47	53	F	Ovary	Adjacent normal ovary tissue	NAT	-
E4	48	41	F	Uterine tube	Uterine tube tissue	Normal	-
E5	49	38	F	Breast	Cancer adjacent breast tissue	AT	-
E6	50	21	F	Uterus	Endometrial tissue	Normal	-

E7	51	47	F	Cervix	Cervical tissue	AT	-
E8	52	45	M	Heart	Cardiac muscle tissue	Normal	-
E9	53	76	F	Eye	Adjacent normal choroidal tissue	NAT	-
E10	54	42	F	Striated muscle	Mesothelium and skeletal muscle tissue	Normal	-
E11	55	0.21	M	Skin	Skin tissue of scalp	Normal	±
F1	56	43	M	Prostate	Prostate tissue	Normal	-
F2	57	71	M	Penis	Cancer adjacent penis tissue	AT	-
F3	58	36	F	Ovary	Ovary tissue	Normal	-
F4	59	15	F	Uterine tube	Uterine tube tissue	Normal	-
F5	60	30	F	Breast	Breast tissue	AT	-
F6	61	40	F	Uterus	Endometrial tissue	Normal	-
F7	62	47	F	Cervix	Cervical tissue	Normal	-
F8	63	35	M	Heart	Cardiac muscle tissue	Normal	-
F9	64	63	M	Eye	Skeletal muscle tissue	NAT	-
F10	65	33	M	Lung	Mesothelium and lung tissue	Normal	-
F11	66	18	F	Skin	Skin tissue of scalp	Normal	±

Table 2. Anti-SSTR2 mAb targeted 1st and 2nd domains of human SSTR2 and mouse SSTR2.

SSTR2 surface receptor	Human sequence	Mouse sequence	Similarity (%)
1st Extra. domain (33-44)	QTEPYYDLTSNA	QTEPYYDLTSNA	100
2nd Extra. domain (104-118)	ALVHWPFGKAICRVV	ALVHWPFGKAICRVV	100

Table 3. PK modeling parameters.

PK Parameters	Calculated Values
Half life $t_{1/2}$ (day)	1.38-2.33
Volume of distribution V_d (mL/kg)	63.05-94.42
Clearance C_L (mL/day/kg)	28.01-37.45
Bioavailability F (%)	568.58-1293.26
Calculated recommended dose D (mg/kg BW)	3.78-14.30
Calculated recommended dosing interval τ (days)	4.40-9.10

Figure Legends

Figure 1. Tissue microarray (TMA) showing strong SSTR2 expression in patients. (**A**) H&E staining of the TMA including human pancreatic NET tissues (columns 2-9, *n* = 38) and normal tissues (control, column 1, *n* = 5). (**B**) An IHC analysis of the TMA showed positive staining for SSTR2. Scale bar equals to 20 μm. The 71% of these cores were positive for SSTR2 and showed strong membrane localization.

Figure 2. Our anti-SSTR2 antibody uniquely binds to NET cells but no or very low binding to normal organs or tissues as validated by immunohistochemistry. (**A1**) Negative or very low surface SSTR2 staining in 33 normal human organs (US Biomax, FDA662a, *n* = 2) representing the cerebrum, cerebellum, peripheral nerve, adrenal gland, thyroid gland, spleen, thymus, bone marrow, lymph node, tonsil, pancreas, liver, esophagus, stomach, small intestine, colon, lung, salivary, pharynx, kidney, bladder, testis, prostate, penis, ovary, uterine tube, breast, endometrium, cervix, cardiac muscle, skeletal muscle, mesothelium, and skin. (**A2**) Positive SSTR2 staining on the cell surface in pancreatic NET patient tissues (*n* = 12). (**B**) Representative high-resolution IHC imaging of cerebellum, cerebrum, liver, lung, muscle, skin, tonsil, prostate, pancreas, and pancreatic NET. Scale bar equals to 50 μm.

Figure 3. Anti-SSTR2 mAb development and production. (**A**) Rank of top anti-SSTR2 mAb clones based on the titer in ELISA screening (data represent mean ± SEM, *n* = 3). (**B**) Evaluation of top 4 clones using flow cytometry. (**C**) SDS-PAGE confirmed the integrity and purity of mAb (M: marker; 1-4: Clones 1-4). (**D**) Evaluation of SSTR2 binding of Clone #4 in control cell lines (WI38 and 917) and NET cell lines (BON and QGP). (**E**) mAb production and hybridoma cell growth in fed-batch suspension cultures (data represent mean ± SEM, *n* = 3). Viable cell density (VCD): ▲, cell viability: Δ, specific growth rate (μ): □.

Figure 4. *In vitro* evaluation of surface binding by our anti-SSTR2 mAb. (**A**) Live-cell CLSM dynamic imaging showing anti-SSTR2 mAb quickly and effectively bound to BON cell surface within 60 mins, followed by internalization within 70 mins. Two-color CLSM: whole cell labeled with GFP (displayed as blue) and SSTR2 mAb-MMAE labeled with AF647 (red). (**B**) Flow cytometry showing our anti-SSTR2 mAb bound to BON cells at a high level and did not bind to the SSTR2 negative control and our mAb had much higher binding percentage than commercial mAb. Stained with 1 μg of mAb-AF647/million cells on ice for 30 mins. (**C**) The AF647-mAb were internalized in three NE cancer cells (green), including BON, TT and MZ. Scale bar equals to 5 μm.

Figure 5. *In vivo* evaluation of NET targeting by our anti-SSTR2 mAb. (**A**) *In vivo* imaging with IVIS showing our mAb could specifically target s.c. NET xenograft in mouse model. The anti-SSTR2 mAb was labelled with fluorescent dye Cy7 and purified using Protein A column. Total of 50 μg Cy5.5-mAb was intravenously (i.v.) injected through tail vein. IVIS images were taken at 24 hr post Cy5.5-mAb injection. (**B**) Our mAb targets both human NET (BON) xenografted tissue and mouse MTC tissues (*n* = 3-4).

Figure 6. ADC construction and *in vitro* characterization. (**A**) Molecule structure of anti-SSTR2 mAb-MMAE using re-bridging linker which maintains the integrity of mAb. (**B**) MS demonstrating the right structure and proper conjugation of linker-MMAE drug in terms of three

product formats. (**C**) The IC_{50} anti-cancer toxicity of free drug (●), ADC constructed using commercial anti-SSTR2 mAb (R&D Systems, ▲), and ADC constructed using our anti-SSTR2 mAb (■) (data represent mean ± SEM, $n = 3$). (**D**) SDS-PAGE gel showing good integrity of mAb-MMAE. (**E**) Western blotting reveling that both anti-SSTR2 mAb and ADC inhibited the proliferation signaling pathways (AKT, Cyclin D1 and P21) while not change SSTR2 surface expression. (**F**) The MMAE drug caused microtubule de-polymerization in BON cell line. Scale bar equals to 20 µm.

Figure 7. MTD and PK study and effect on brain of ADC in s.c. PanNET xenografted mouse models. (**A**) MTD studies that test the effect of five ADC dosages including 4, 8, 12, 16 and 20 mg/kg-BW show no negative effect on mice weight and behaviors and maximal dosage was not reached ($n = 2$). (**B**) H&E staining showing ADC treatment did not change brain morphology and had no damage to brain. Scale bar equals to 200 µm. (**C**) PK studies show the stability and kinetics parameters of ADC (data represent mean ± SEM, $n = 4$).

Figure 8. Anti-NET efficacy study of ADC in PanNET (BON-Luc) xenografted models. (**A**) Tumor volume changes after Bon-Luc cell injection and treatment (data represent mean ± SEM, $n = 6$). Tumor was measured with calipers, and calculated as ellipsoid. Black arrow indicating ADC (8 mg/kg BW) treatment date. (**B**) Tumor fluorescence flux measurement with IVIS image system (data represent mean ± SEM, $n = 6$). (**C**) Tumor bearing mice harvested. (**D**) Weight of the tumors excised from harvested mice on Day 29. (**E**) Body weight of the mice during treatment. ▲: treatment group injected with ADC, ●: control group injected with mAb, and ■: control group injected with saline. (**F**) Western blotting of tumors from represented mice ($n = 3$). (**G**) Anti-SSTR2 IHC staining of the saline and ADC treated tumors. (**H**) H&E staining of Saline or ADC treatment tumor. Scale bar equals to 50 µm. *** $p \leq 0.001$.

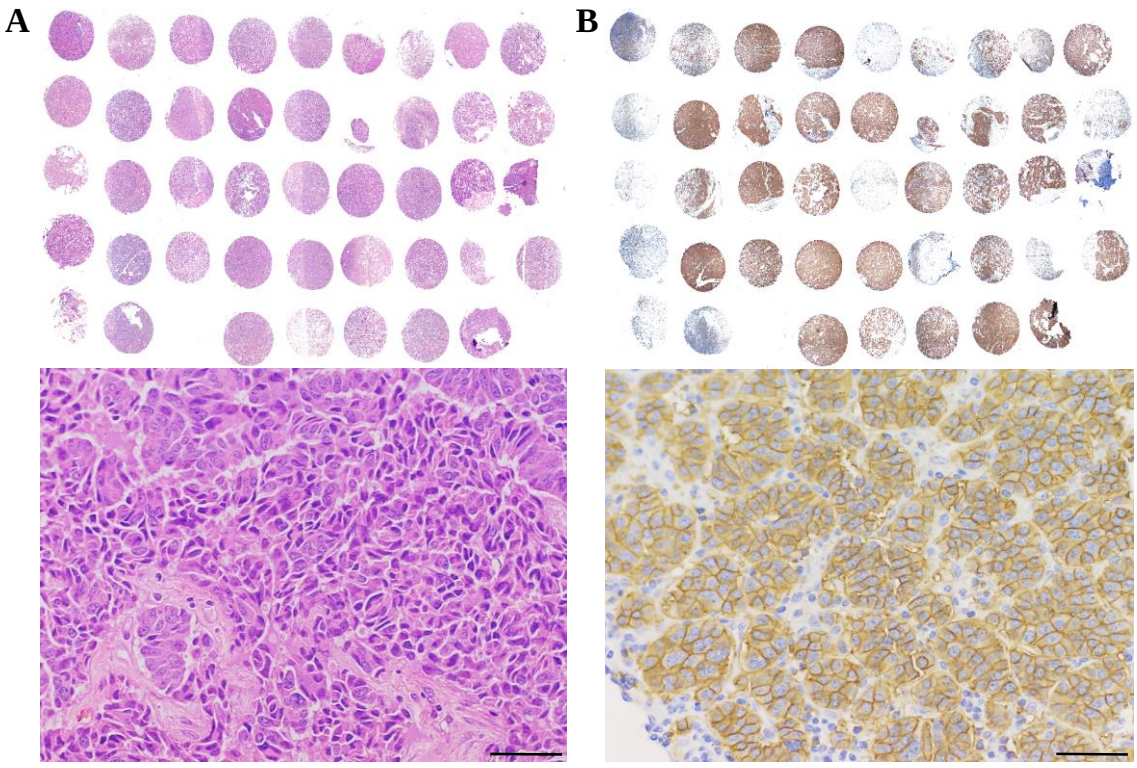

Figure 1. Tissue microarray (TMA) showing strong SSTR2 expression in patients.

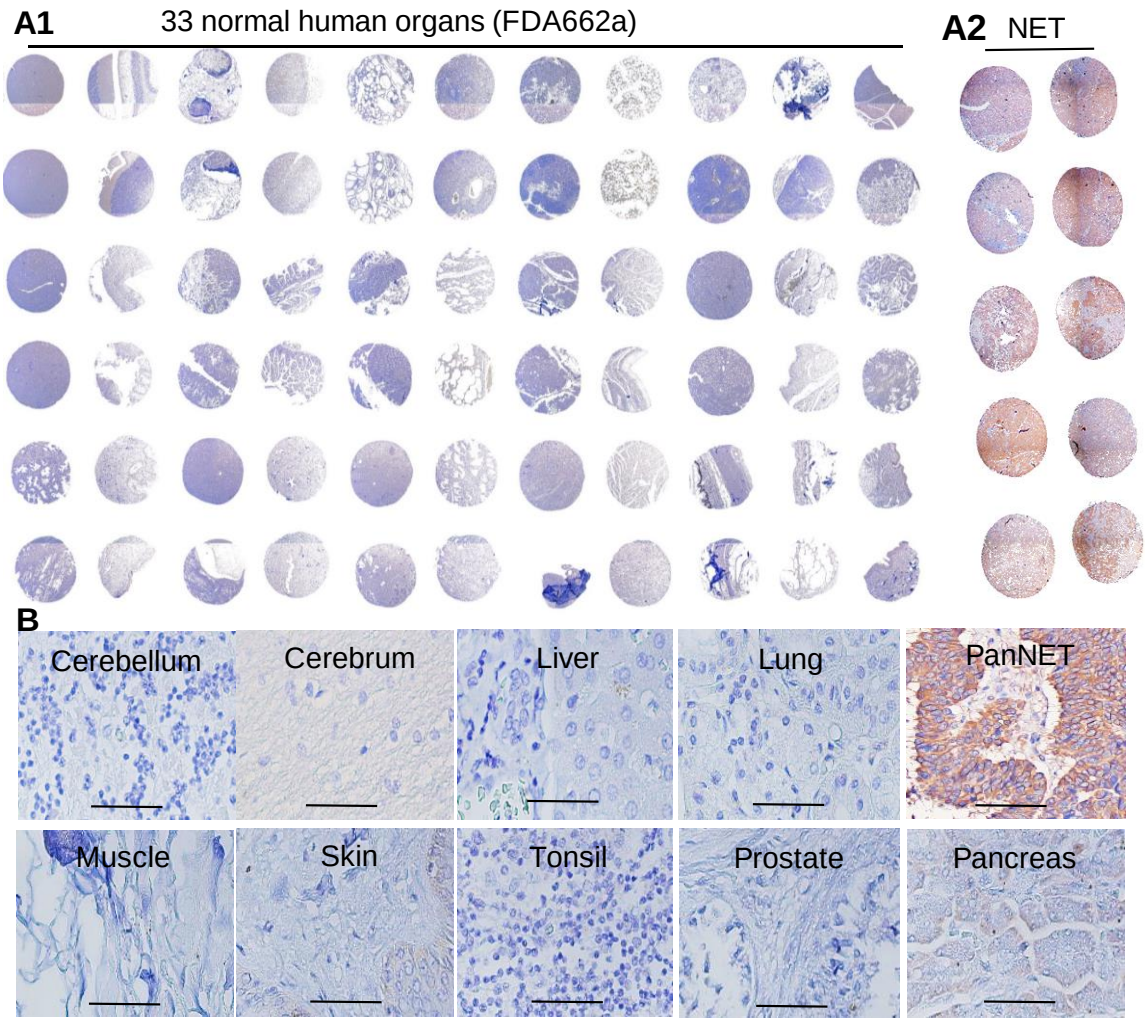

Figure 2. Our anti-SSTR2 antibody uniquely binds to NET cells but no or very low binding to normal organ tissues as validated by immunohistochemistry.

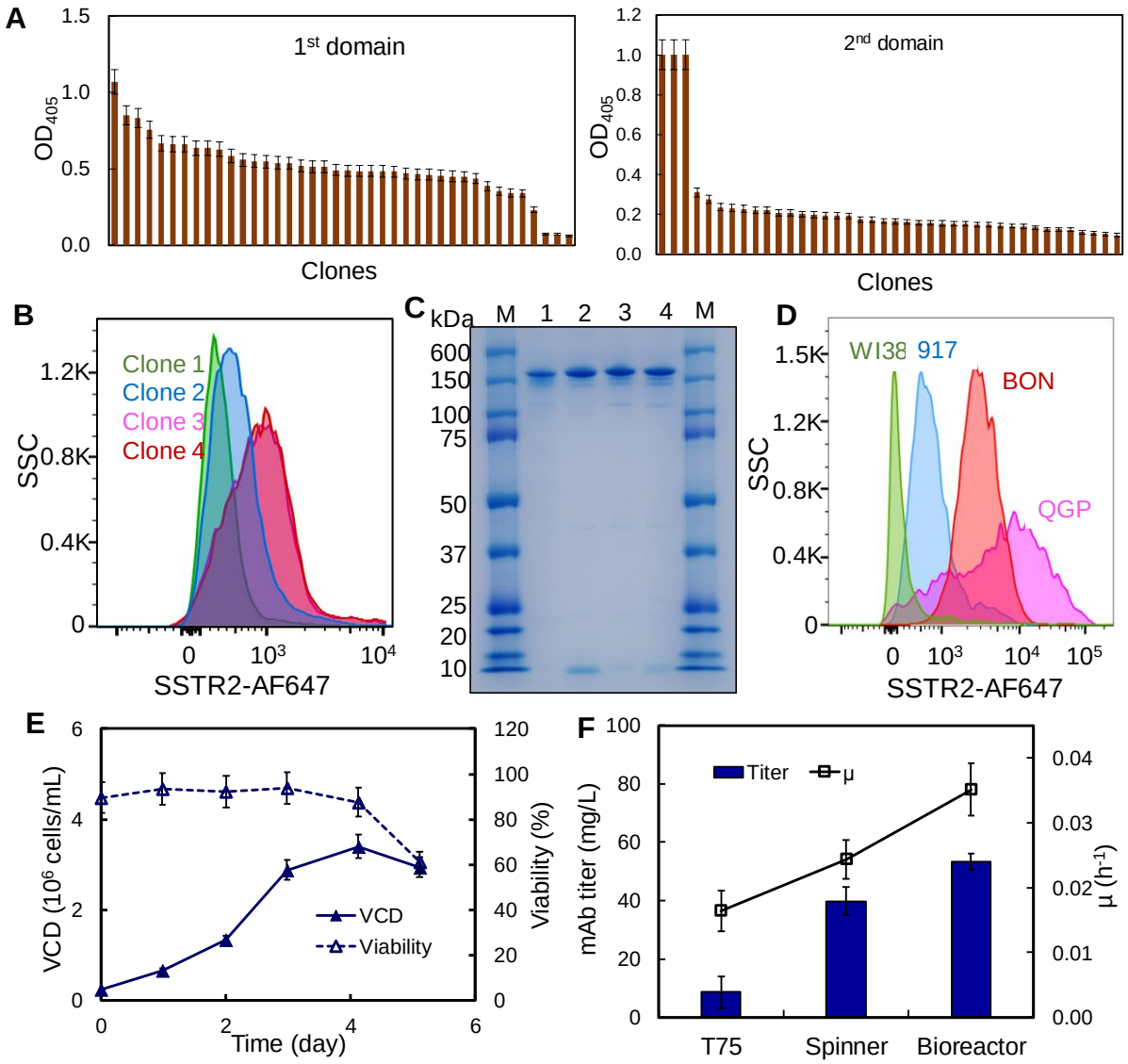

Figure 3. Anti-SSTR2 mAb development and production.

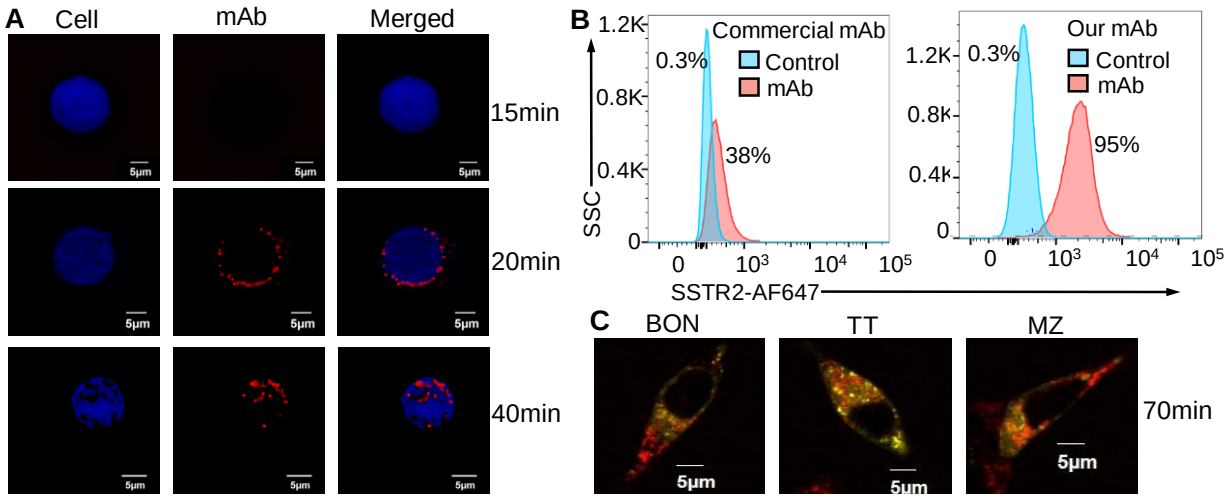

Figure 4. *In vitro* surface binding evaluation of our anti-SSTR2 mAb.

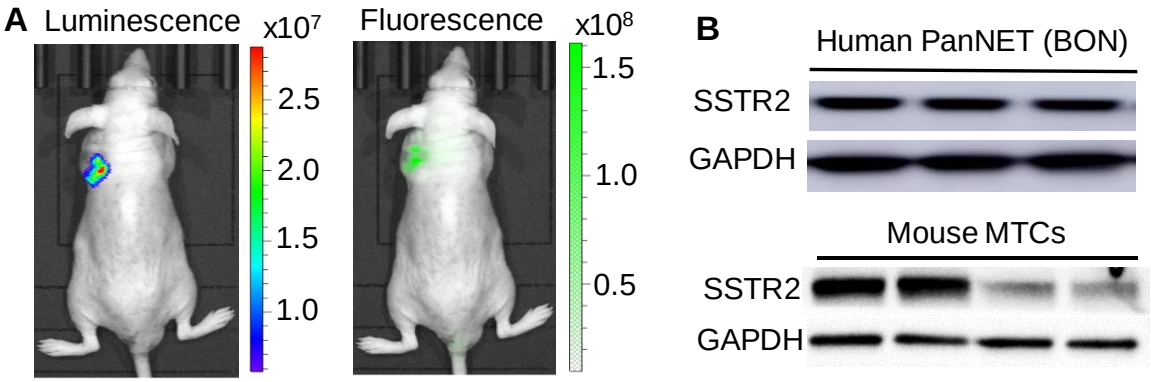

Figure 5. *In vivo* evaluation of NET targeting by our anti-SSTR2 mAb.

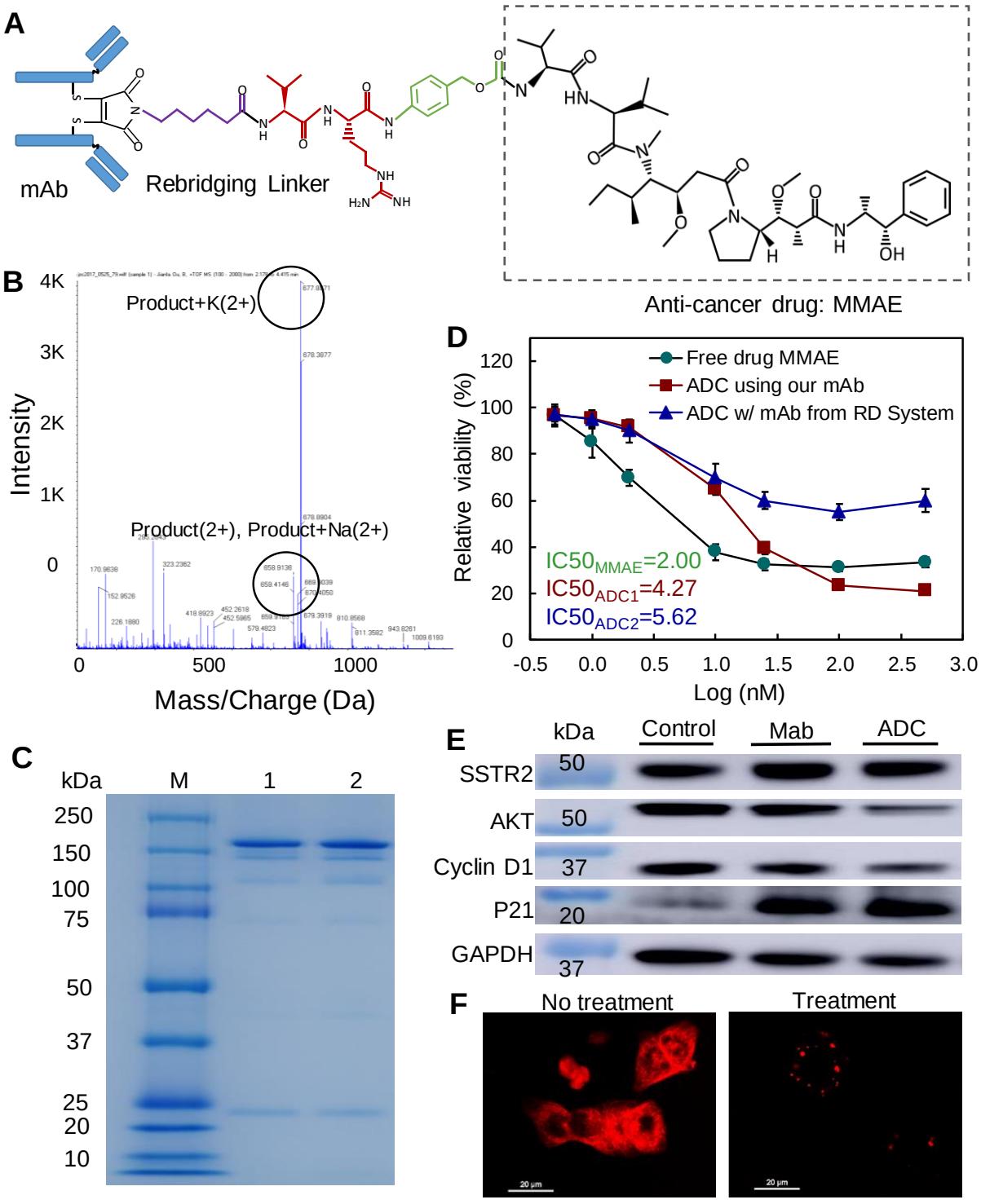

Figure 6. ADC construction and *in vitro* characterization.

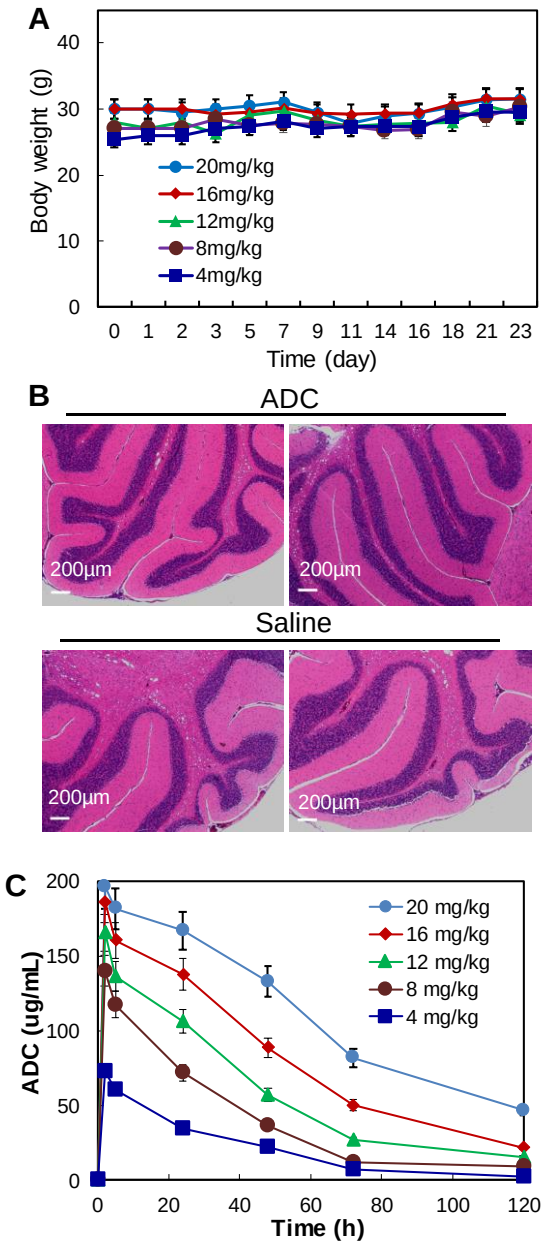

Figure 7. MTD and PK study and effect on brain of ADC in PanNET xenograft models.

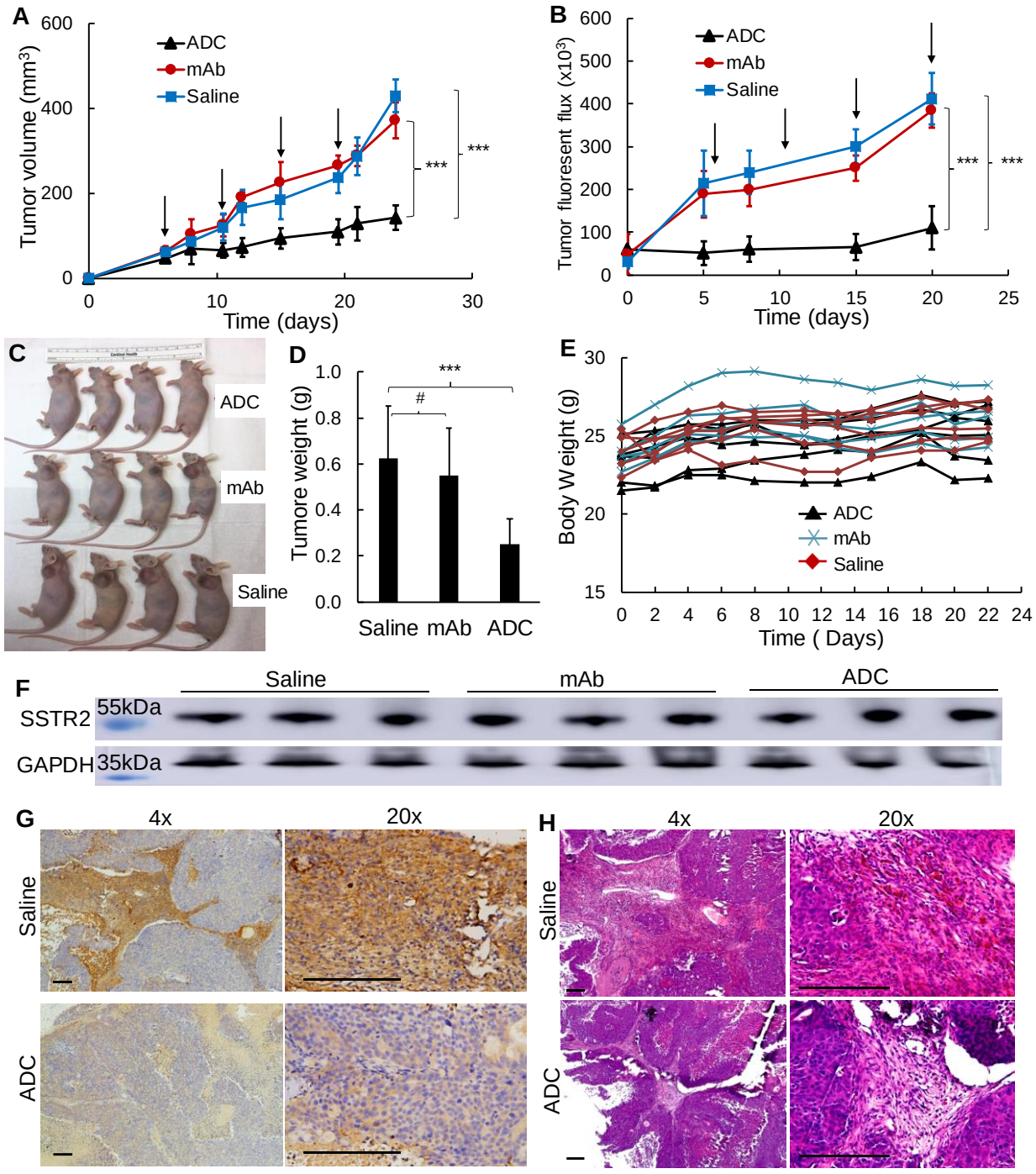

Figure 8. Anti-NET efficacy study of ADC in PanNET (BON-Luc) xenografted models.